PHYSICOCHEMICAL PROBLEMS
OF MATERIALS PROTECTION

Theoretical Prediction and Experimental Study of Benzimidazole Derivate as a Novel Corrosion Inhibitor for Carbon Steel in 1.0 M HCl

Y. El Aoufir[a, b], J. Sebhaoui[c], H. Lgaz[a, d], Y. El Bakri[c], A. Guenbour[b],
F. Bentiss[e, f], A. Zarrouk[g, *], E.M. Essassi[c], and H. Oudda[a]

[a]Laboratoire de Chimie Organique, Inorganique, Electrochimie et Environnement, Ecole Supérieure d'éducation et de la Formation, Ibn Tofail University, PB 133-14050, Kenitra, Morocco

[b]Laboratory of Materials, Nanotechnology and Environment, Mohammed V University, Faculty of Sciences, P.O. Box. 1014, Rabat, Morocco

[c]Laboratoire de chimie organique heterocyclique, URAC 21, Pôle de compétence pharmacochimie, Université Mohammed V, Faculté des sciences, Rabat, Maroc

[d]Laboratory of Applied Chemistry and Environment, ENSA, Ibn Zohr University, PO Box 1136, Agadir, 80000 Morocco

[e]Laboratoire de Catalyse et de Corrosion des Matériaux (LCCM), Faculté des Sciences, Université Chouaib Doukkali, B.P. 20, El Jadida, M-24000 Morocco

[f]Lille University, ENSCL, UMET CNRS UMR 8207, Lille, F-59000 France

[g]Laboratory of Materials, Nanotechnology, and Environment, Mohammed V University, Faculty of Sciences, P.O. Box. 1014, Rabat, Morocco

*e-mail: azarrouk@gmail.com

Abstract—The inhibiting effect of benzimidazole derivate (DBI) on corrosion of carbon steel (CS) at temperature range of 303−333 K was investigated in hydrochloric acid by DC potential dynamic polarization and AC electrochemical impedance spectroscopy. It was found that this compound behaved as a mixed-type inhibitor with predominantly cathodic effect. The EIS results indicate that the inhibition efficiency increases with increasing the inhibitor concentration and the maximum inhibition (%) was obtained in the presence of 10^{-3} M of DBI. The adsorption of DBI on the carbon steel surface is described by the Langmuir adsorption isotherm and had a physical and chemical mechanism. The results found experimentally were corroborated by DFT-quantum chemical calculations and molecular dynamics simulations (MDS) methods.

1. INTRODUCTION

Corrosion of metals is reckoned amongst the most significant and challenging problems in industry. Carbon steel (CS) is used in mass amounts in marine applications, chemical processing, petroleum production and refining, storage tanks, reaction vessels, chemical batteries, construction, and metal processing equipment. Hydrochloric acid (HCl) solutions commonly used throughout pickling, industrial acid cleaning, acid de-scaling, and oil well acidifying processes cause corrosion of steel. Thereby, the use of corrosion inhibitors increases continually to protect the metal from corrosion by development of inhibiting films [1−6]. The mechanism of their action can be different, depending on the metal, the medium and the structure of the inhibitor substance. The performance of the organic corrosion inhibitor substances containing heteroatoms shows promising results. Nevertheless, the stability of the inhibitor film formed over the

metal surface depends on some physicochemical properties of the molecule, related to its electronegative functional groups (CO, NH, OH and CS) [7−10], electron rich aromatic systems [11−13], the possible steric effects, electronic density of donors, type of the corrosive medium and nature of the interaction between the p-orbital of inhibitors with the d-orbital of iron [14−17]. So, the benzimidazole and its derivatives have received considerable attention on their inhibition properties for metallic corrosion of mild/carbon steel over the past year [18, 19]. They found that these compounds have fairly good inhibiting properties for steel corrosion in acid medium.

Although the experimental techniques have shown that the inhibitory substances act by adsorption at the metal interface, the mechanism of protection of organic corrosion inhibitor molecules has not been accurately understood. Actually, little attention has been paid to how these organic surface modifiers bind
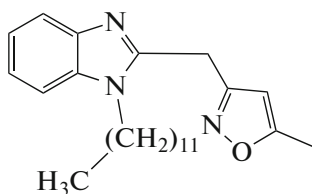
Fig. 1. The chemical structure of 1-dodecyl-2-[(5-methyl-isoxazol-3-yl)-methyl]-benzimidazole.

to metal surfaces, and why seemingly minor modifications in the structures of organic active compounds can have a profound effect on their effectiveness. The evolution in computer simulation methods hold promise that questions regarding the inhibitive properties of such compounds can be addressed at the atomic level. Therefore, there is a wealth of theoretical studies concerning the associations between molecular mechanism and inhibition effect [20].

The aim of this work is to study the effect of benzimidazole derivate on inhibition properties on the corrosion of Carbon steel in 1 M HCl by using electrochemical methods. Invaluable quantum chemical parameters such as E_{HOMO} (highest occupied molecular orbital energy), E_{LUMO} (lowest unoccupied molecular orbital energy) and Fukui indices calculations were obtained by using $DMol^3$ module, help to understand the adsorption properties by considering the structure of 1-dodecyl-2-[(5-methyl-isoxazol-3-yl)-methyl]-benzimidazole (DBI) (Fig. 1).

2. EXPERIMENTAL

2.1. Synthesis of Corrosion Inhibitor

1,5-Benzodiazepine derivatives are a raw material in obtaining various heterocyclic systems. Authors of [21] have obtained isoxazolyl-methylbenzimidazole from the action of hydroxylamine hydrochlorideon 4-(2-oxo-propylidene)-1,5-benzodiazepin-2-one (Azzaoui et al. 2006). We took over the same method for the preparation of the new derivative 1-dodecyl-2-[(5-methyl-isoxazol-3-yl)-methyl]-benzimidazole (**2**) from 1-dodecyl-4-(2-oxopropylidene)-2,3,4,5-tetrahydro-1 H-1,5-benzodiazepin-2-one (**1**). Scheme 1
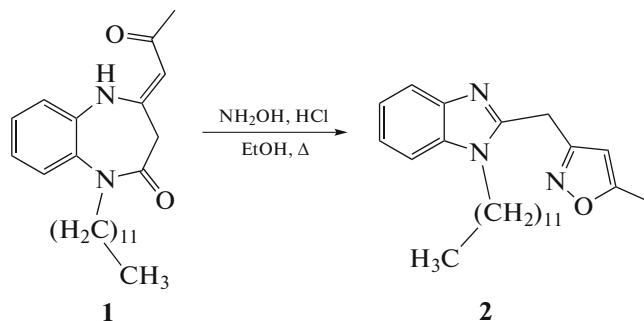
Scheme 1

A mixture of 1-dodecyl- 2-[(5-methyl-isoxazol-3-yl)-methyl]-benzimidazole (10 mmol) and hydroxylamine hydrochloride (10 mmol) in ethanol was refluxed for a period of 2h. After neutralization with NaHCO₃, the residue formed was recrystallized from hexane to afford **2** as a dark brown solid.

¹H-NMR, (DMSO-d6): 0.82(s,3H,CH₃), 1.19(s,18H,CH₂), 1.59(q,2H,CH₂),4.14(t,2H;CH₂-N), 6.14(s,1H,CH), 7.10-7.53(4H,CH_aromatique) (d ppm): ¹³C-NMR (DMSO-d6) (d ppm): 12.19(CH₃), 14.40(CH₃), 31.75-22.55(CH₂-aliph), 43.62 (C−N), 115(C−CH₃), 135.53-102.87(C_aromatique), 160(C=N), 169.96(C=C).

2.2. Test Solution and Material

An aggressive solution of hydrochloric acid of 1.0 M concentration was prepared by dilution with double distilled water of 12.076 M HCl (analytical grade). The concentration of inhibitor used was varied from 10^{-6} to 10^{-3} M, and the volume of the electrolyte employed was 80 mL in all studies. The carbon steel C35 used had the following chemical composition (wt %): 0.370 C, 0.230 Si, 0.680 Mn, 0.016 S, 0.077 Cr, 0.011 Ti, 0.059 Ni, 0.009 Co, 0.160 Cu and balance Fe.

2.3. Electrochemical Studies of Corrosion Inhibition

The experimental device allowing the plotting of the polarization curves and impedance diagrams is a Voltalab PGZ 100 potentiostat/galvanostat driven by a computer and associated with "Voltamaster 4" software. For all the tests we used a thermostated double cell wall (Tacussel type CEC/TH) containing three electrodes; a working electrode consisting of a carbon steel. The latter is disposed opposite the platinum auxiliary electrode and a saturated calomel KCl electrode (SCE) as the reference electrode. The electrode is maintained at its free corrosion potential for 30 min under normal aeration conditions. The measurements are carried out at 303 K in a 1 M solution of dilute

hydrochloric acid. The intensity-potential curves are obtained with a scanning speed of 0.5 mV/s. The recording of these curves takes place within a potential interval of between −800 and −200 mV/SCE. The measurement of the electrochemical impedances was carried out under the same conditions as the plotting of the polarization curves at frequencies between 100 kHz and 10 mHz exercising a sinusoidal perturbation potential of 10 mV.

For DC technique, the inhibition efficiency (η%) was defined as:

$$\eta_{\text{Tafel}}(\%) = \frac{I_{\text{corr}}^{\circ} - I_{\text{corr}}^{i}}{I_{\text{corr}}^{\circ}} \times 100, \tag{1}$$

where I_{corr}° and I_{corr}^{i} are the corrosion current density values without and with inhibitor [22].

For AC-impedance, the inhibiting efficiency η_Z is also calculated using the equation (2):

$$\eta_Z(\%) = \frac{R_{\text{ct}}^{i} - R_{\text{ct}}^{\circ}}{R_{\text{ct}}^{i}} \times 100. \tag{2}$$

Where, R_{ct}° and R_{ct}^{i} are the charge transfer resistance in absence and in presence of inhibitor, respectively.

2.4. Quantum Chemical Calculations

E_{HOMO} is the highest occupied molecular orbital energy, E_{LUMO} is the lowest unoccupied molecular orbital energy and Fukui indices calculations were executed utilizing *DMol³* module in Materials Studio version 6.0 [23]. These calculations employed an *ab initio*, gradient-corrected functional (*GGA*) method with a double numeric plus polarization (DNP) basis set and a Becke One Parameter (BOP) functional. It is well-known that the phenomena of electrochemical corrosion appear in aqueous phase. *DMol³* includes certain COSMO controls, which allow for the treatment of solvation effects [24, 25].

2.5. Monte Carlo Simulation Study

The Monte Carlo (MC) search was adopted to compute the low configuration adsorption energy of the interactions of the DBI on a clean iron surface. The Monte Carlo (MC) simulation was carried out exploitating Materials Studio 6.0 software (Accelrys, Inc.). Detail theoretical procedures using Monte Carlo methodology are well documented previously [26−28].

3. RESULTS AND DISCUSSION

3.1. Polarization Study

Figure 2 shows the DC-technique for the corrosion of CS in 1.0 M HCl solution without and with addition of different concentrations of DBI at 303 K. The cor-
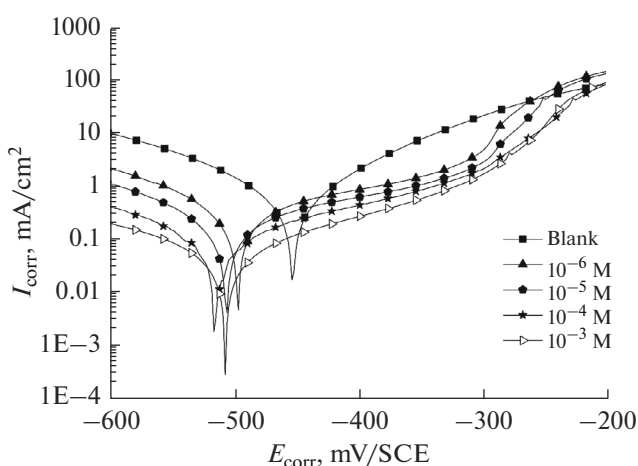

Fig. 2. Anodic and cathodic polarization curves for the corrosion of CS in 1.0 M HCl in the absence and presence of different concentrations of DBI.

rosion electrochemical parameters such as corrosion potential symbolized by E_{corr}, corrosion current density (I_{corr}), anodic Tafel slope (β_a), cathodic Tafel slope (β_c) and the inhibitory efficacy (η%) were determined and gathed in Table 1.

It is clear from Fig. 2 that the anodic and cathodic current densities decrease effectively when the concentration of DBI in the acid solution increases and generally with a slight shift in the E_{corr} values towards negative potentials, suggesting that the inhibitor molecule retard the corrosion process. In the acidic media in our study (hydrochloric acid solution), oxidative dissolution of CS in the anodic region and hydrogen reduction in the cathodic region are observed in the Tafel plots. In addition, the parallel cathodic Tafel curves in Fig. 1 show that the hydrogen evolution is activation-controlled and the reduction mechanism is not touched by the presence of DBI [29].

In Fig. 2 the anodic branch of polarization curves, at the polarization initial stage, the current densities increased slowly and anodic polarization was enhanced predominantly with the polarization potential shifting positively, which signify that the adsorption process dominates the anodic reaction and the adsorption rate is higher than the desorption rate of DBI molecule on CS surface. However, for polarization potential higher than 300 mV/SCE, desorption of DBI was visible, and the current density also increased markedly in comparison with that at the anodic scan initial stage [30]. The phenomenon may be due to the significant dissolution of metal, leading to some desorption of DBI molecules from the electrode surface [31, 32]. This result shows that the inhibition effect of this compound depends on the electrode potential.

From the results depicted in Table 1, it is clear that the values of I_{corr} decrease considerably with increas-

Table 1. The electrochemical parameters calculated by using the potentiodynamic polarization technique for the corrosion of CS in 1.0 M HCl in the absence and presence of different concentrations of DBI at 303 K

Medium	Concentration, M	$-E_{corr}$, mV/SCE	I_{corr}, μA cm^{-2}	β_a, mV dec^{-1}	$-\beta_c$, mV dec^{-1}	η, %
Blank	1.0	452.0	507	100	122	—
DBI	10^{-6}	495.3	127	72.1	56.7	74.9
	10^{-5}	504.7	81	70.0	59.5	84.0
	10^{-4}	514.9	50	70.9	60.0	90.1
	10^{-3}	506.1	34	98.3	103.5	93.3

ing of the concentration of DBI. This observation proposes that the rate of CS dissolution was retarded by the formation of a protective inhibitor film on the metal surface, and this protective film creates a barrier on the interface metal/solution. The corrosion potentials shift to negative values in the presence of DBI. Furthermore, the cathodic and anodic Tafel slopes modify with concentration, the observed behaviors indicate that DBI acts as the mixed type corrosion inhibitor with predominantly cathodic effect [33–35]. According to the polarization measurements, the inhibitory efficacy increases with increasing of concentration of DBI and attain a maximum value of 93.24% at 10^{-3} M.

3.2. Electrochemical Impedance Spectroscopy (EIS)

EIS can give more details about corrosion mechanisms. The Mechanistic information can be derived from the impedance diagram forms. The representative Nyquist of CS electrode in 1.0 M HCl solution in the absence and presence of various concentrations of DBI at corrosion potential is represented in Fig. 3.

The impedance parameters obtained for DBI molecules are given in Table 2.

The results confirm that DBI effectively inhibited the corrosion of CS in 1.0 M HCl. An important change in the corrosion behavior of carbon steel can be observed from the impedance responses after the addition of DBI in 1.0 M HCl solution. This is attributed to increasing of DBI concentration that leads to an increase in surface coverage and an increase in diameter of the loops. Adsorbed DBI molecules form a protective film which protects the CS surfaces and inhibits the corrosion of metal.

The Nyquist diagrams in Fig. 3 show single semicircles with centers below the real impedance, revealing that the dissolution of CS in the studied electrolyte systems is controlled by single charge transfer process. The Nyquist diagrams in the absence and presence of DBI are characterized by one capacitive loop. The capacitive loops are not perfect semicircles because of heterogeneity and irregularity of the carbon steel surface [36].

In this case, the standard Randle's circuit model of Fig. 4, which has been previously used to model the
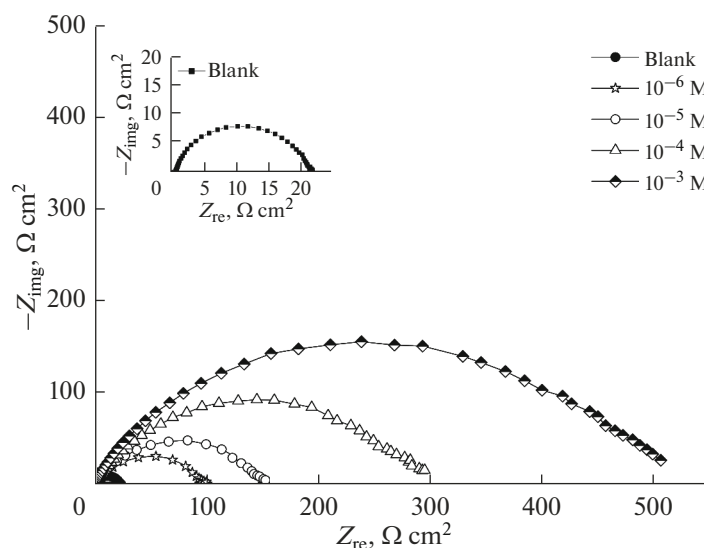

Fig. 3. Nyquist plots for carbon steel in 1.0 M HCl solution without and with different concentration of DBI at 303K.

Table 2. Impedance parameters recorded for carbon steel electrode in 1.0 M HCl solution in the absence and presence of DBI at 303K

Medium	Concentration, M	R_s, Ω cm²	R_{ct}, Ω cm²	$10^{-4}Q$, Ω⁻¹cm⁻²s⁻ⁿ	n	C_{dl}, μF cm⁻²	τ, s	η_Z, %
Blank	1.0	0.568	20.24	2.420	0.860	112.04	0.00227	—
DBI	10^{-6}	0.869	95.76	2.21	0.70	42.34	0.00405	79.0
	10^{-5}	1.102	147	1.11	0.71	36.61	0.00538	86.3
	10^{-4}	0.649	285.2	1.0	0.71	23.86	0.00680	92.9
	10^{-3}	0.202	486	0.80	0.72	14.47	0.00703	95.8

iron/acid interface [37, 38], fits well our experimental results. Figure 4 shows the suitable equivalent circuite, comprises parallel combination of the charge transfer resistance (R_{ct}) and the constant phase element (CPE), both in series with the solution resistance (R_s). CPE is introduced in place of pure double layer capacitance (C_{dl}) to give more accurate fit as the double layer at interface does not react as ideal capacitor. The CPE impedance is given by the following relation [39]:

$$Z_{CPE} = A^{-1} (i\omega)^{-n}. \tag{3}$$

Where, A is the CPE constant, x is the angular frequency (in rad s⁻¹), $i^2 = 1$ (the imaginary number) and n is a CPE exponent that can be used as a gauge of the non- homogeneity of the surface.

It can be seen from Table 2 that charge transfer resistance increases considerably after the addition of DBI to the corrosive solution, while C_{dl} decreases. These observations can be explaining by the formation of insulating protective film of the inhibitors at the metal/solution interface [40, 41].

The relaxation time (τ) of a surface state is the time needed for the return of the charge distribution to equilibrium after an electrical disturbance. In the case when no distributed element is introduced to replace the double-layer capacitance, it is defined [42] as (4):

$$\tau = R_{ct}C_{dl}. \tag{4}$$

In this investigation, the additions of DBI caused an increase in τ values, signifying that the charge and discharge rates to the metal-solution interface are greatly decreased.

The single maximum obtained in Bode phase angle plots (Figs. 5a, 5b) confirmed the presence of one time constant at intermediate frequencies, broadening of this maximum in the presence of inhibitors accounts for the adsorption of DBI on the electrode surface [43, 44]. The magnitude of impedance in the presence of DBI is important than in the absence of DBI and the value of impedance increases on increasing the concentration of DBI suggested that the corrosion rate is reduced in the presence of the DBI.

Electrochemical impedance spectroscopy results (η %) are in good agreement with the results (η %) obtained by potentiodynamic polarization method.

3.3. Adsorption Isotherm

On the basis of evaluation of the interaction between the inhibitors and steel surface, it is important to consider the adsorption isotherms to analyze the mechanism and nature of the adsorption processes of chemicals species on the CS surface [45]. For the studied organic inhibitor substance, it was found that the experimental data obtained from polarization readings could be fitted by Langmuir's adsorption isotherm. According to this isotherm, the surface coverage (θ) is related to inhibitor concentration (C) by using the equation (5) [46]:

$$\frac{\theta}{1-\theta} = K_{ads}C. \tag{5}$$

Rearranging equation gives (6):

$$\frac{C}{\theta} = \frac{1}{K_{ads}} + C. \tag{6}$$

Where θ is the surface coverage, K_{ads} is the equilibrium constant of the DBI adsorption process, C is the concentration of DBI and θ is the surface coverage. A fitted straight line is obtained for the plot of C/θ versus C with slope close to 1 as seen in Fig. 6. The strong correlation ($R^2 > 0.999$) indicates that the adsorption of DBI inhibitor on the carbon steel surface obeyed this isotherm. Langmuir isotherm arrogates that the adsorbed molecules occupy only one site and there are no interactions with other adsorbed species [47].
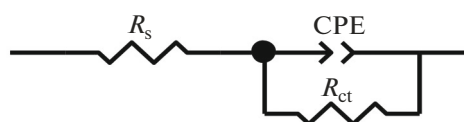
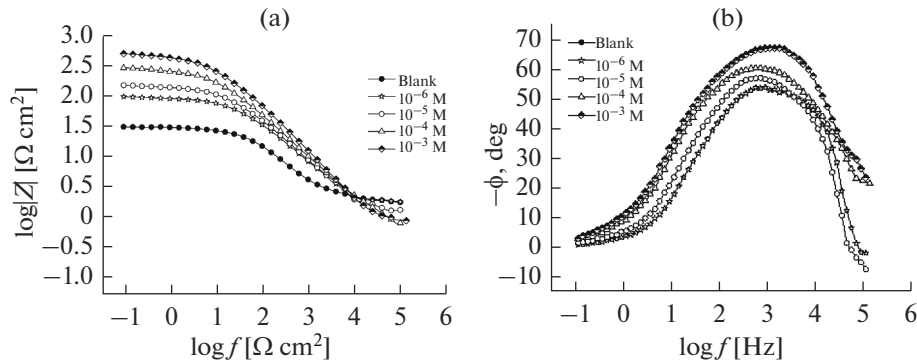**Fig. 4.** Equivalent circuit used to fit the EIS data.

Fig. 5. Bode diagrams (a) and phase angle (b) for carbon steel in 1.0 M HCl without and with DBI at 303K.

Large value of K_{ads} obtained for DBI inhibitor implies more efficient adsorption and hence better corrosion inhibition efficiency. Using the value of K_{ads} and value of ΔG°_{ads} are evaluated by [48]:

$$\Delta G^{\circ}_{ads} = -RTLn(55.5K_{ads}). \quad (7)$$

Where R is the gas constant equal to 8.314 J mol^{-1} K^{-1}, T is the absolute temperature expressed in Kelvin and the value of 55.5 is the concentration of H_2O in solution in mol/L. The thermodynamic parameters (K_{ads} and ΔG°_{ads}) are displayed in Table 3. The negative sign of the Gibbs free energy of adsorption reveals the adsorption of inhibitor onto the metal surface [47]. The calculated value of ΔG_{ads} is around −39 kJ/mol, which may indicate that the adsorption mechanism of DBI on CS is complex mixed type adsorption (chemisorption and physisorption) [49].
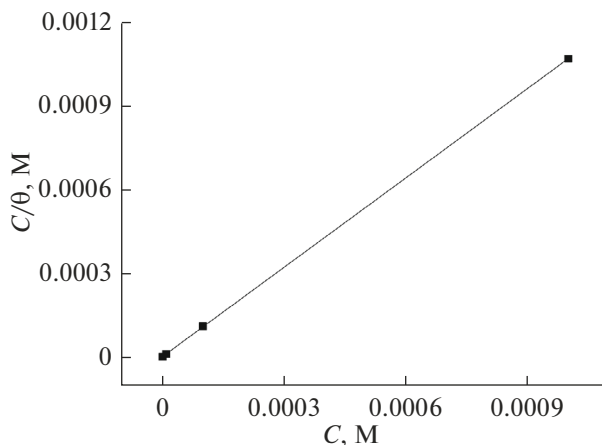

Fig. 6. Langmuir adsorption isotherm (C/θ vs. C) of DBI in 1.0 M HCl

3.4. Effect of Temperature

The variation of the corrosion density with the temperature was investigated in 1.0 M HCl, both in absence and presence of DBI. For this objective, polarization readings were performed at temperatures between 303 and 333 k in absence (Fig. 7a) and presence of 10^{-3}M of DBI (Fig. 7b). The electrochemical parameters such as corrosion density (I_{corr}), corrosion potential (E_{corr}), surface coverage (θ) and $\eta\%$ are shown in Table 4.

Although, Table 4 data clearly shows an increase in corrosion rate with increasing of the temperature, however the corrosion rate in the presence of DBI solutions is always lower than the blank one. It is seen also that the investigated DBI inhibitor have been inhibiting properties at all temperatures studied and the values of inhibitory efficacy remain slightly constant with temperature increase.

Activation thermodynamic parameters were utilized to give some insight about the inhibition mechanism and adsorption mechanism. It has been observed that I_{corr} depends of temperature and this temperature dependency can be expressed using Arrhenius (8):

$$Ln(I_{corr}) = LnA + \left(\frac{-E_a}{RT}\right). \quad (8)$$

Where E_a is the apparent activation energy expressed in kJ/mol, R is the universal gas constant (8.314 J/K mol), T is the absolute temperature (K), and A is the Arrhenius preexponential factor. The Arrhenius plot for CS corrosion in absence and presence of optimum concentration of DBI is shown in Fig. 8. The values of the activation energies are listed in Table 5. It is clear for this Table that the values of E_a for the CS dissolution in presence of DBI were higher than that in their absence. This increase in the E_a suggests the physisorption that occurs during first stage of adsorption processes [50]. Further, increase in E_a value signifies that DBI decrease the CS dissolution by increasing the energy barrier for corrosion process [51, 52].

Table 3. Equilibrium adsorption parameters for adsorption DBI on carbon steel surface in 1.0 M HCl solution

Inhibitor	R^2	Slope	K_{ads}, M^{-1}	$-\Delta G^{\circ}_{ads}$, kJ mol^{-1}
DBI	0.9998	0.98896	128158.3	39.74

Table 4. Electrochemical parameters and the corresponding inhibition efficiencies at various temperature studied of carbon steel in 1.0 M HCl in absence and presence 10^{-3}M of DBI

| Medium	Temperature, K	$-E_{corr}$, mV/SCE	I_{corr}, µA cm^{-2}	η, %
Blank	303	452.0	507	—
	313	454.0	860	—
	323	443.0	1840	—
	333	450.0	2800	—
DBI	303	506.1	34	93.3
	313	515.8	126	85.3
	323	527.1	287	84.4
	333	531.5	495	82.3

An alternative formulation of Arrhenius equation is (9) [53]:

$$I_{corr} = \frac{RT}{Nh}\exp\left(\frac{\Delta S_a}{R}\right)\exp\left(\frac{-\Delta H_a}{RT}\right). \quad (9)$$

Where h is Planck's constant, N is Avogadro's number, ΔS_a is the entropy of activation and ΔH_a is the enthalpy of activation. Figure 10 shows a plot of Ln (I_{corr}/T) vs. $1/T$. Straight lines are obtained with a slope of $\Delta H_a/R$ and an intercept of Ln($R/Nh + \Delta S_a/R$) from whichthe values of ΔS_a and ΔH_a are calculated and are given in Table 5. Examination of these data revealed that the thermodynamic parameters (ΔS_a and ΔH_a) for dissolution reaction of CS in 1.0 M HCl in the presence of DBI are higher than that obtained in

the absence of DBI. The positive sign of ΔH_a reflects that the adsorption of DBI used is endothermic [54]. On comparing the values of the entropy of activation ΔS_a given in Table 5, it is clear that entropy of activation increased positively in the presence of DBI than in corrosive solution. The increase of ΔS_a value reveals that an increase in disordering takes place on going from reactant to the activated complex [54].

3.5. Quantum Chemical Calculations

3.5.1. Global molecular reactivity. In order to analyze the effect of molecular structure and also electronic parameters on DBI inhibitor performance the quantum chemical calculations were performed [55].
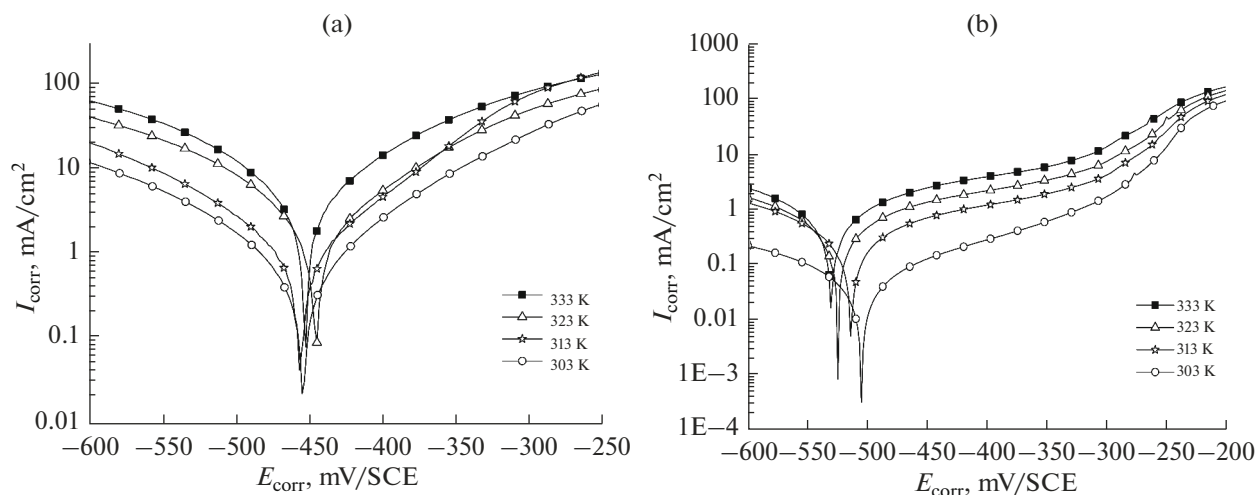
Fig. 7. Effect of temperature on the behavior of carbon steel/1.0 M HCl interface in (a) uninhibited solution, (b) at 10^{-3}M of DBI.
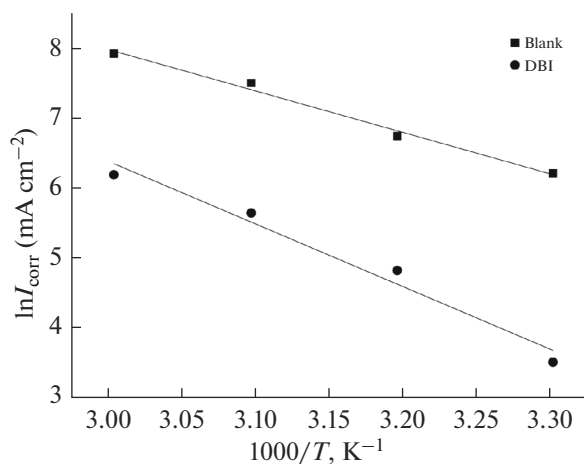
Fig. 8. Ln I_{corr} vs. 1000/T for carbon steel dissolution in 1.0 M HCl in the absence and presence 10^{-3}M of DBI.
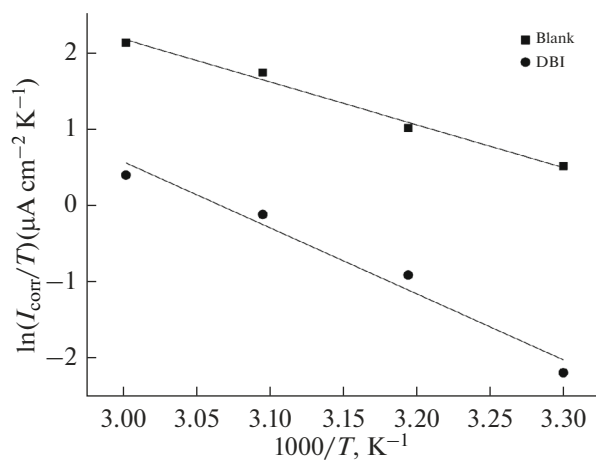

Fig. 9. Transition state plot of carbon steel in 1.0 M HCl solution without and with the addition of 10^{-3}M of DBI.

Quantum chemical parameters obtained from the calculations which are responsible for the inhibitory efficacy of DBI such as the energy of highest occupied molecular orbital (E_{HOMO}), energy of lowest unoccupied molecular orbital (E_{LUMO}), HOMO−LUMO energy gap (ΔE) and the fraction of electrons transferred (ΔN) have been listed in Table 6. In addition, Fig. 10 illustrates the optimized molecular structure, HOMO and LUMO orbitals of DBI.

From the Fig. 10 it can be seen that the electron density of both HOMO and LUMO are localized principally on the π-bonds and heteroatoms which indicates that the heteroatoms of DBI could be both the acceptor and the donor of the electron. According to the frontier molecular orbital theory (FMO) of chemical reactivity, the formation of a transition state is due to an interaction between the frontier orbitals (HOMO and LUMO) of reacting species. Hence, only the HOMO and LUMO of both reactants are considered when analyzing the chelation processes of adsorption [56−58]. The difference between the energy levels of these orbitals is important in the evaluation of inhibitory efficacy. The littler the orbital energy gap (ΔE) between the participating HOMO and LUMO, the stronger are the interactions between two reacting species which cause the adsorption of the inhibitor substance on the metal surface [59].

The results in Table 6, explain the better inhibitive properties of tested compound. The DBI contain heteroatoms and double bonds in their molecular structure, which favorite the interactions between these

actives centers and the metal surface. On the other hand, It is well reported that the alkyl chain length increase the inhibition efficiency of an organic compound [60] which further support the good inhibitive performance of DBI. The electron affinity (EA) and ionization potential (IP) are deduced from E_{HOMO} and E_{LUMO} by the Eqs. (10) and (11):

$$IP = -E_{HOMO}, \tag{10}$$

$$EA = -E_{LUMO}. \tag{11}$$

Mulliken electronegativity (χ) and Absolute hardness (η) can be approximated using [61, 62]:

$$\chi = \frac{IP + EA}{2}, \tag{12}$$

$$\eta = \frac{IP - EA}{2}. \tag{13}$$

The fraction of electrons (ΔN) transferred can be evaluated by Pearson electronegativity scale:

$$\Delta N = \frac{\phi - \chi_{inh}}{2(\eta_{Fe} + \eta_{inh})}. \tag{14}$$

Where ϕ is the work function of the iron surface with the value of 4.06 eV for Fe (1 1 0) [63], χ_{inh} is the absolute electronegativity associated to the inhibitor molecule, $\eta_{Fe} = 0$ and η_{inh} are the absolute hardness of metal and the inhibitor molecule, respectively. Values of ΔN exhibit inhibitive performance resulted from electrons donations. If $\Delta N < 3.6$, the inhibitory efficacy increases with the increase in electron-donation

Table 5. Thermodynamic parameters for adsorption of DBI on carbon steel surface in 1.0 M HCl. Solutions

Medium	E_a, kJ mol^{-1}	ΔH_a, kJ mol^{-1}	ΔS_a, mol^{-1} K^{-1}
Blank	49.41	46.77	−39.06
DBI	74.67	72.03	23.38

Table 6. The computed quantum chemical parameters for DBI compound

Quantum parameters	E_{HOMO}, eV	E_{LUMO}, eV	ΔE_{gap}, eV	ΔN
Value	−5.085	−1.687	3.398	0.198

ability to the metal surface [64]. In this paper, there is a good correlation between inhibitory efficacy and the parameter of ΔN.

3.5.2. Fukui functions. Fukui function is necessary in understanding the local site selectivity. The Fukui function $(f(\vec{r}))$ is defined as [65]:

$$f(\vec{r}) = \left(\frac{\partial \rho(\vec{r})}{\partial N}\right)_{V(\vec{r})}. \qquad (15)$$

Table 7. Fukui indices of the investigated compound

Atom	f_k^+	f_k^-
C (1)	0.011	0.021
C (2)	−0.002	0.018
C (3)	0.001	0.023
C (4)	0.004	0.038
C (5)	0.009	0.019
C (6)	0.007	0.020
N (7)	0.024	0.195
C (8)	−0.024	0.088
N (9)	0.002	0.029
C (10)	−0.006	−0.025
C (11)	0.006	−0.012
C (12)	−0.009	−0.010
C (13)	−0.011	−0.013
C (14)	−0.006	−0.005
C (15)	0.010	−0.005
C (16)	−0.001	−0.008
C (17)	−0.001	−0.002
C (18)	−0.007	−0.004
C (19)	−0.003	−0.003
C (20)	−0.004	−0.004
C (21)	−0.003	−0.002
C (22)	−0.009	−0.016
C (23)	0.071	−0.007
N (24)	0.174	0.006
O (25)	0.087	0.014
C (26)	0.127	0.012
C (27)	0.040	0.001
C (28)	−0.030	−0.005

The nucleophilic attack Fukui function (f_k^+) and electrophilic attack Fukui function (f_k^-) can be calculated as [66]:
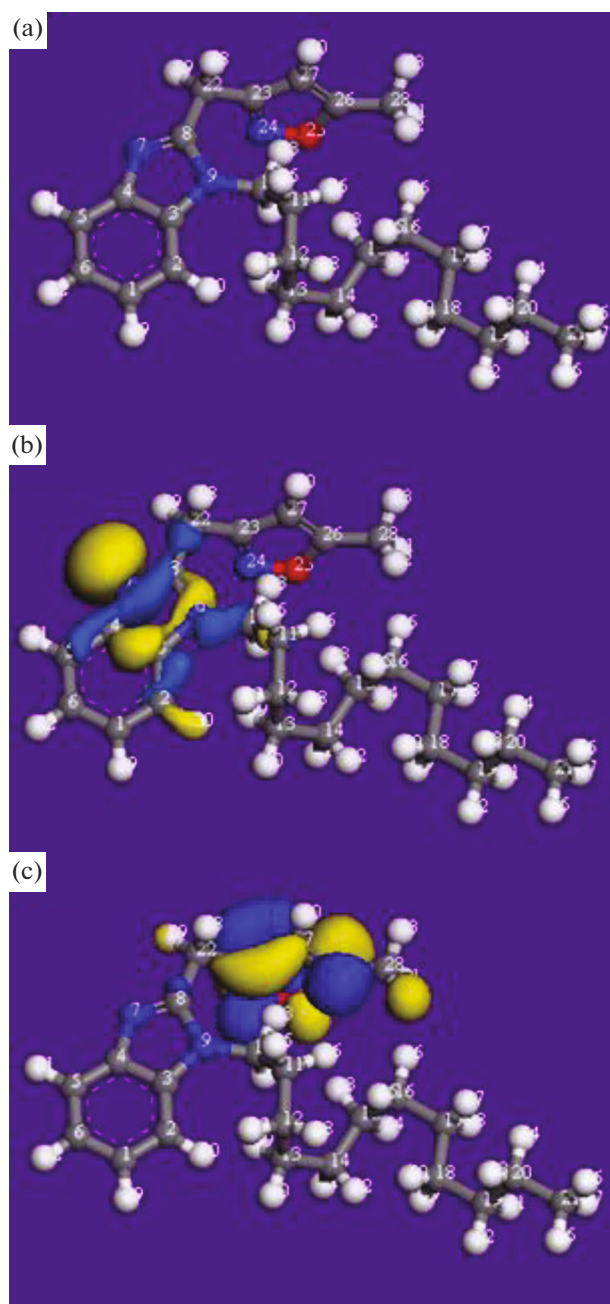
Fig. 10. Optimized molecular structure of DBI (a), HOMO (b) and LUMO (c) orbitals.
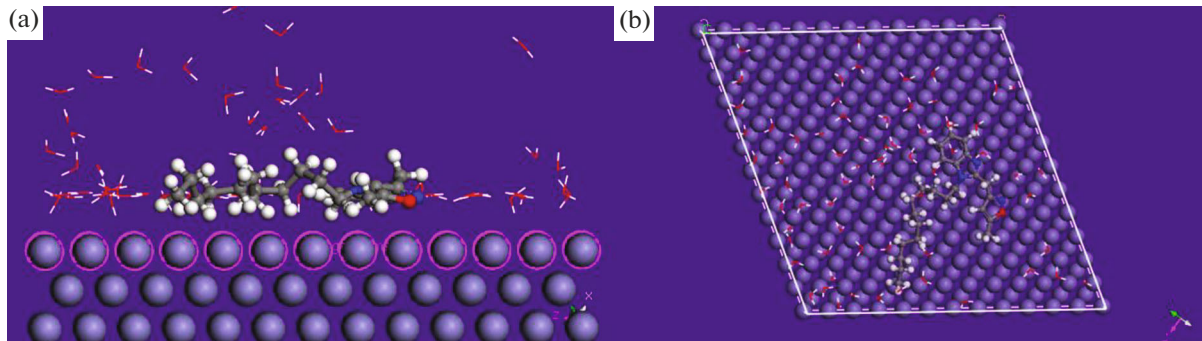
Fig. 11. The most stable low energy configuration for the adsorption of the inhibitor on Fe (1 1 0) surface obtained through the Monte Carlo simulation (a) side view, (b) top view.

$$f_k^+ = q_k \left(N + 1 \right) - q_k \left(N \right), \qquad (16)$$

$$f_k^- = q_k \left(N \right) - q_k \left(N - 1 \right). \qquad (17)$$

Where $q_k \left(N + 1 \right)$, $q_k \left(N \right)$, $q_k \left(N - 1 \right)$ are charge values of atom k for cation, neutral and anion, respectively.

The values of f_k^+ and f_k^- are also given in Table 7. Generally, high values of f_k^+ and f_k^- mean the high capacity of the atom to gain and lost electron, respectively. For the nucleophic attack, the most reactive sites are N (24), O (25) and C (26), which can accept electrons from metal surface to form back-donating bond. On the other hand, the values of f_k^- indicate that they will happen on the N (7) and C (8); which can denote electrons to metal surface to form coordinate bond.

3.6. Monte Carlo Simulations

Nowadays, molecular dynamics simulation has been extensively used to describe the interactions between the inhibitor and metal surface [67, 68]. In our present study the Monte Carlo simulation calculation was used to find the lowest energy for the DBI/Fe (110) system. The outputs and descriptors calculated by the Monte Carlo simulation, such as the total adsorption, adsorption energy, rigid adsorption and deformation energies are listed in Table 8. Figure 11 represents the most stable low energy configuration for the adsorption of DBI on Fe(110) surface obtained through the Monte Carlo simulations. It is evident from Fig. 11 that the DBI molecule adsorbed on a par-

allel orientation on the iron surface to maximize surface coverage and contact. This ensures strong interaction and by extension high inhibition action observed experimentally. It has been reported that the more negative the adsorption energy, the stronger the adsorbate-metal interaction [61]. It is clear from Table 8, that DBI gave the strong negative adsorption energy. Therefore, DBI is expected to exhibit greater inhibition abilities

4. CONCLUSIONS

The benzimidazole compound has been tested as corrosion inhibitor for carbon steel protection in 1.0 M HCl solution. The results illustrated that tested compound acts as the mixed type corrosion inhibitor with predominantly cathodic effect. The detailed studies of DBI showed that the corrosion inhibition efficiency of this compound increases with increasing inhibitor concentration and attain 95.8% at 10^{-3}M. EIS studies revealed that the studied compound formed a protective surface film at metal/electrolyte interface. The inhibition efficiency was decreased modestly with increasing temperature. Adsorption of the DBI molecule on the carbon steel obeyed the Langmuir isotherm and thermodynamic data extracted by this isotherm explains physical and chemical adsorption. Quantum chemical calculations indicated that the inhibition is achieved more through the active sites of present inhibitor. Monte Carlo simulations showed that the inhibitor adsorb on a parallel orientation on the iron surface.

Table 8. Outputs and descriptors calculated by the Monte Carlo simulation for the lowest adsorption configurations of DBI on Fe (110) surface (in kcal/mol)

Total energy	Adsorption energy	Rigid adsorption energy	Deformation energy	DBI : dEad/dNi	H$_2$O : dEad/dNi
−1464	−1471	−1502	31.14	−245.84	−0.73

REFERENCES

1. Guadalupe, Hernández J., García-Ochoa, E., Maldonado-Rivas, P.J., Cruz, J., and Pandiyan, T., *J. Electroanal. Chem.,* 2011, vol. 655, p. 164.

2. Saravanamoorthy, S. and Velmathi, S., *Prog. Org. Coat.,* 2013, vol. 76, p. 1527.

3. Khaled, K.F., *Electrochim. Acta,* 2009, vol. 54, p. 4345.

4. Solmaz, R., Kardas, G., Yazici, B., and Erbil, M., *Colloids Surf., A,* 2008, vol. 312, p. 7.

5. Bentiss, F., Lagrenée, M., and Traisnel, M., *Corros. Sci.,* 2000, vol. 56, p. 733.

6. Bentiss, F., Traisnel, M., and Lagrenée, M., *J. Appl. Electrochem.,* 2001, vol. 31, p. 41.

7. Popova, A., Sokolova, E., Raicheva, S., and Christov, M., *Corros. Sci.,* 2003, vol. 45, p. 33.

8. Ozcan, M., Dehri, I., and Erbil, M., *Appl. Surf. Sci.,* 2004, vol. 236, p. 155.

9. Hosseini, M.G., Mertens, S.F.L., Ghorbani, M., and Arshadi, M.R., *Mater. Chem. Phys.,* 2003, vol. 78, p. 800.

10. Bilgic, S. and Calickan, N., *Appl. Surf. Sci.,* 1999, vol. 152, p. 107.

11. Emregul, K.C., Kurtaran, R., and Atakol, O., *Corros. Sci.,* 2003, vol. 45, p. 2803.

12. Gomma, G.K. and Wahdan, M.H., *Mater. Chem. Phys.,* 1995, vol. 39, p. 209.

13. Wang, X., Wan, Y., Zeng, Y., and Gu, Y., *Int. J. Electrochem. Sci.,* 2012, vol. 7, p. 2403.

14. EL Aoufir, Y., Lgaz, H., Bourazmi, H., Kerroum, Y., Ramli, Y., Guenbour, A., Salghi, R., El-Hajjaji, F., Hammouti, B., and Oudda, H., *J. Mater. Environ. Sci.,* 2016, vol. 7, p. 4330.

15. Cruz, J., Pandiyan, T., and García-Ochoa, E., *J. Electroanal. Chem.,* 2005, vol. 583, p. 8.

16. Cruz, J., Martinez-Aguilera, L.M.R., Salcedo, R., and Castro, M., *Int. J. Quantum Chem.,* 2001, vol. 85, p. 546.

17. EL Aoufir, Y., Lgaz, H., Toumiat, K., Salghi, R., Jodeh, S., Zougagh, M., Guenbour, A., and Oudda, H., *Res. J. Pharm., Biol. Chem. Sci.,* 2016, vol. 7, p. 1219.

18. Zhang, J., Yu, W., Yu, L., Yan, Y., Qiao, G., Hu, S., and Ti, Y., *Corros. Sci.,* 2011, vol. 53, p. 1331.

19. Pauline, S.A., Sahila, S., Gopalakrishnan, C., Nanjundan, S., and Rajendran, N., *Prog. Org. Coat.,* 2011, vol. 72, p. 443.

20. Awe, F.E., Idris, S.O., Abdulwahab, M., and Oguzie, E.E., *Cogent Chem.,* 2015, vol. 1, p.1112676.

21. El-Azzaoui, B., Rachid, B., Doumbia, M.L., Essassi, E.M., Gornitzka, H., and Bellan, J., *Tetrahedron Lett.,* 2006, vol. 47, p. 8807.

22. Negm, N.A., Elkholy, Y.M., Zahran, M.K., and Tawfik, S.M., *Corros. Sci.,* 2010, vol. 52, p. 3523.

23. *Materials Studio 2013, Revision 6.0,* San Diego, CA: Accelrys Inc., 2013.

24. Delley, B., *J. Chem. Phys.,* 1990, vol. 92, p. 508.

25. Delley, B., *J. Chem. Phys.,* 2000, vol. 113, p. 7756.

26. Eivani, A.R., Zhou, J., and Duszczyk, J., *Comput. Mater. Sci.,* 2012, vol. 54, p. 370.

27. Hmamou, D.B., Salghi, R., Zarrouk, A., Zarrok, H., Touzani, R., Hammouti, B., and El Assyry, A., *J. Environ. Chem. Eng.,* 2015, vol. 3, p. 2031.

28. Kaya, S., Tüzün, B., Kaya, C., and Obot, I.B., *J. Taiwan Inst. Chem. Eng.,* 2016, vol. 58, p. 528.

29. Döner, A., Sahin, E.A., Karda, G., and Serindag, O., *Corros Sci.,* 2013, vol. 66, p. 278.

30. El Bribri, A., Tabyaoui, M., Tabyaoui, B., El Attari, H., and Bentiss, F., *Mater. Chem. Phys.,* 2013, vol. 141, p. 240.

31. Khaled, K.F. and Al-Qahtani, M.M., *Mater. Chem. Phys.,* 2009, vol. 113, p. 150.

32. El mehdi, B., Mernari, B., Traisnel, M., Bentiss, F., and Lagrenee, M., *Mater. Chem. Phys.,* 2003, vol. 77, p. 489.

33. Zheng, X., Zhang, S., Li, W., Yin, L., He, J., and Wu, J., *Corros. Sci.,* 2014, vol. 80, p. 383.

34. Ansari, K.R., Quraishi, M.A., and Singh, A., *Corros. Sci.,* 2014, vol. 79, p. 5.

35. Wang, X., Yang, H., and Wang, F., *Corros. Sci.,* 2011, vol. 53, p. 113.

36. Ramesh, S. and Rajeswari, S., *Electrochim. Acta,* 2004, vol. 49, p. 811.

37. Ashassi-Sorkhabi, H., Shaabani, B., and Seifzadeh, D., *Appl. Surf. Sci.,* 2005, vol. 239, p. 154.

38. Outirite, M., Lagrenée, M., Lebrini, M., Traisnel, M., Jama, C., Vezin, H., and Bentiss, F., *Electrochim. Acta,* 2010, vol. 55, p. 1670.

39. Xu, F., Duan, J., Zhanga, S., and Hou, B., *Mater. Lett.,* 2008, vol. 62, p. 4072.

40. Pavithra, M.K., Venkatesha, T.V., Kumar, M.K.P., and Tondan, H.C., *Corros. Sci.,* 2012, vol. 60, p. 104.

41. Prabhu, R.A., Venkatesha, T.V., Shanbhag, V., Praveen, B.M., Kulkarni, G.M., and Kalkhambkar, R.G., *Mater. Chem. Phys.,* 2008, vol. 108, p. 283.

42. Popova, A., Christov, M., and Vasilev, A., *Corros. Sci.,* 2007, vol. 49, p. 3290.

43. Tang, Y., Zhang, F., Hu, S., Cao, Z., Wu, Z., and Jing, W., *Corros. Sci.,* 2013, vol. 74, p. 271.

44. Singh, A.K., Shuka, S.K., Singh, M., and Quraishi, M.A., *Mater. Chem. Phys.,* 2011, vol. 129, p. 68.

45. Noor, E.A. and Al-Moubaraki, A.H., *Mater. Chem. Phys.,* 2008, vol. 110, p. 145.

46. EL Aoufir, Y., El Bakri, Y., Lgaz, H., Zarrouk, A., Salghi, R., Warad, I., Ramli, Y., Guenbour, A., Essassi, E.M., and Oudda, H., *J. Mater. Environ. Sci.,* 2017, vol. 8, p. 3290.

47. Amar, H., Tounsi, A., Makayssi, A., Derja, A., Benzakour, J., and Outzourhit, A., *Corros. Sci.,* 2007, vol. 49, p. 2936.

48. Avci, G., *Colloids Surf., A,* 2008, vol. 317, p. 730.

49. Singh, A.K., Mohapatra, S., and Pani, B., *J. Ind. Eng. Chem.,* 2016, vol. 33, p. 288.

50. Yadav, D.K., Quraishi, M.A., and Maiti, B., *Corros. Sci.,* 2012, vol. 55, p. 254.

51. Musa, A.Y., Kadheem, A.A.H., Mohamad, A.B., Daud, A.R., Takriff, M.S., and Kamarudin, S.K.A., *Corros. Sci.,* 2009, vol. 51, p. 2393.

52. Krishnegowda, P.M., Venkatesha, V.T., Krishnegow-da, P.K.M., and Shivayogiraju, S.B., *Ind. Eng. Chem. Res.,* 2013, vol. 52, p. 722.

53. Bochris, J.*O'M. and Reddy, A.K.N., Modern Electro-chemistry,* New York: Plenum Press, 1977, vol. 2.

54. Martinez, S. and Stern, I., *Appl. Surf. Sci.,* 2002, vol. 199, p. 83.

55. El Makrini, B., Lgaz, H., Larouj, M., Salghi, R., Rasem Hasan, A., Belkhaouda, M., Jodeh, S., Zou-gagh, M., and Oudda, H., *Pharma Chem.,* 2016, vol. 8, p. 256.

56. Badiea, A.M. and Mohana, K.N., *Corros. Sci.,* 2009, vol. 51, p. 2231.

57. Ma, H., Chen, S., Liu, Z., and Sun, Y., *J. Mol. Struct.: THEOCHEM,* 2006, vol. 774, p. 19.

58. Rastogi, R.B., Jaiswal, V., and Maurya, J.L., *Proc. Inst. Mech. Eng., Part J,* 2014, vol. 228, p. 198.

59. Zhang, J., Liu, J., Yu, W., Yan, Y., You, L., and Liu, L., *Corros. Sci.,* 2010, vol. 52, p. 2059.

60. Stoyanova, A., Petkova, G., and Peyerimhoff, S.D., *Chem. Phys.,* 2002, vol. 279, p. 1.

61. Pearson, R.G., *Inorg. Chem.,* 1988, vol. 27, p. 734.

62. Sastri, V. and Perumareddi, J., *Corros. Sci.,* 1997, vol. 53, p. 617.

63. Lukovits, I., Kalman, E., and Zucchi, F., *Corros. Sci.,* 2001, vol. 57, p. 3.

64. Ju, Z., Kai, P., and Li, Y., *Corros. Sci.,* 2008, vol. 50, p. 865.

65. Parr, G. and Yang, W., *J. Am. Chem. Soc.,* 1984, vol. 106, p. 4049.

66. Hu, Q., Hu, J.C., Fan, C.C., Jia, X.L., Zhang, J., and Guo, W.Y., *Acta Chim. Sin.,* 2010, vol. 68, p. 2051.

67. Sasikumar, Y., Adekunle, A.S., Olasunkanmi, L.O., Bahadur, I., Baskar, R., Kabanda, M.M., Obot, I.B., and Ebenso, E.E., *J. Mol. Liq.,* 2015, vol. 211, p. 105.

68. Shahraki, M., Dehdab, M., and Elmi, S., *J. Taiwan Inst. Chem. Eng.,* 2016, vol. 62, p. 313.